Tu-AM-SSym-1

COMMUNICATION AT THE MOLECULAR LEVEL; WHY DO WE CARE? Robert M. Stroud, Dept. of Biochemistry, University of California, San Francisco, San Francisco, CA 94143.

Tu-AM-SSym-2

THE HUMAN IMMUNODEFICIENCY VIRUS PROTEASE: INHIBITOR BINDING AND STRUCTURAL PLASITICITY. Paula M. D. Fitzgerald, Merck Sharp and Dohme Research Laboratories, P. O. Box 2000, Rahway, New Jersey, USA 07065

The human immunodeficiency virus type 1 (HIV-1) has been shown to be a causative agent of acquired immune deficiency syndrome (AIDS). The HIV-1 genome encodes a protease that catalyses a critical step in the maturation of the virus, making the protease a potential target for therapy in the treatment of AIDS. To assist in the rational design of HIV-1 protease inhibitors, the structure of the protease has been determined by X-ray crystallographic techniques in both an unliganded and an inhibited form.

The structure of the unliganded enzyme was determined by multiple isomorphous replacement techniques and refined at 2.3Å resolution. This structure shows the enzyme to be a dimer in which the active site is formed around the twofold axis by symmetrically disposed residues from each monomer.

Inhibited complexes of the structure were formed by reacting the enzyme with acetyl-pepstatin and with a reduced octapeptide. The acetyl-pepstatin complex structure was determined by molecular replacement techniques and refined at 2.0Å resolution; the reduced peptide complex structure has been refined at 2.5Å resolution. The inhibitor binds in a extended conformation on the surface of the enzyme; its binding is stabilized by interaction with residues in the so-called "flaps" of the enzyme. Residues in the flap change position by as much as 7 Å between the free enzyme and the inhibited complexes. Smaller structural rearrangements occur throughout the enzyme structure.

In the complex structures, portions of the protease dimer deviate significantly from twofold symmetry, generating an asymmetric dimer. The binding of acetyl-pepstatin appears to be insensitive to this asymmetry, as the molecule binds in both possible directions. The binding of the reduced peptide, however, is sensitive to the asymmetry, as the predominant mode of binding is unidirectional.

Tu-AM-SSym-3

HOW MUSCLES WORK OR THE PAIN OF THE LONG DISTANCE RUNNER. Roger Cooke, University of California, San Francisco, San Francisco, CA 94143.

Tu-AM-SSym-4

CAREERS IN BIOPHYSICS. Norma M. Allewell, Dept. of Molecular Biology & Biochemistry, Wesleyan University, Middletown, CT 06457.

Tu-Am-A1

THE PHOTOSYNTHETIC REACTION CENTER POLYPEPTIDE FROM *HELIOBACILLUS MOBILIS* CONTAINS THE HIGHLY CONSERVED CYSTEINE-CONTAINING REGION FOUND IN PHOTOSYSTEM I

J.T. Trost, D. C. Brune, U. Liebl, W. Vermaas, and R. E. Blankenship
Center for the Study of Early Events in Photosynthesis
Arizona State University, Tempe, AZ 85287-1604, U.S.A.

The photosynthetic reaction center was isolated from *Heliobacillus mobilis* as described by Trost & Blankenship (*Biochemistry*, **28**, 9898-9904). The major 47kM$_r$ polypeptide was then isolated in milligram quantities by preparative SDS-PAGE and subjected to enzymatic cleavage with trypsin, chymotrypsin, V8 protease and clostripain. Chemical cleavage with cyanogen bromide and BNPS-skatole was also performed. Only clostripain and cyanogen bromide in 70% trifluoroacetic acid gave significant cleavage of the polypeptide. The products of cleavage were separated by SDS-PAGE, blotted onto Immobilon-P and sequenced on an automated gas phase sequencer.

Three sequences of greater than 20 residues were obtained from the clostripian digested polypeptide and one sequence from the cyanogen bromide treatment. When the sequences were compared to all protein sequences and deduced protein sequences from the GenBank library only one showed any significant homology. The alignment is shown below. Surprisingly, the sequence lined up with the highly conserved cysteine containing region found in photosystem I from plants and cyanobacteria. The cysteine sulfurs in PS I are proposed as ligands to iron-sulfur center F_X. This result further supports the idea that the photosynthetic reaction center from Heliobacteria is similar to PS I.

```
            550        560        570        580
PS I        DKKDFGYSFPCDGPGRGGTCDISAWDAFYLAVFWMLNT
H.mobilis         DGEFPCLGPAYGGTCSISLVDQF
```

Sequence alignment of a clostripain generated fragment from *H. mobilis* with the PS I A2 polypeptide from tobacco. Cysteines are shown as bold, exact matches are underlined and conservative replacements as italic.

The protein sequences obtained have been used to design oligonucleotide probes for the polymerase chain reaction to amplify part of the reaction center gene(s). A single DNA fragment of approximately 500 bp was produced. Southern blots of restriction fragments of *H. mobilis* genomic DNA probed with the radiolabeled PCR product show specific hybridization to single major bands under the stringent conditions used. This does not necessarily indicate that there is only one reaction center gene in the Heliobacteria. Currently the reaction center gene is being cloned and the sequenced. The obtained gene will then be used under less stringent conditions to determine if there is more than one gene for the large reaction center polypeptide in the Heliobacteria.

Tu-AM-A2

QUENCHING OF CHLOROPHYLL EXCITED STATES BY QUINONES: APPLICATION TO THE STUDY OF EXCITED STATE TRANSFER DYNAMICS IN PHOTOSYSTEM I PIGMENT-PROTEIN COMPLEXES

James Weifu Lee, Warren Zipfel and Thomas G. Owens
Section of Plant Biology, Cornell University, Ithaca, NY 14853

Some substituted benzoquinones and naphthoquinones are able to quench chlorophyll excited states (excitations) in photosynthetic antenna systems without affecting the primary photochemical reactions, and have been widely used in the study of photosystem II (PS II) fluorescence. We are exploring applications of these type of quinones to studies of excitation transfer dynamics in the antenna chlorophylls of PS I. Our studies show that 5-OH-naphthoquinone has a strong quenching effect in isolated PS I complexes, which can be detected by both steady state fluorescence and P700 photooxidation kinetic measurements. Theoretical treatment of modified Stern-Volmer analysis in photosynthetic antennae shows that the effects of quinone quenching on fluorescence and P700 photooxidation can provide information on the site of quinone interaction and on the overall excitation transfer dynamics. The Stern-Volmer quenching constant (K_{SV}) gives the binding affinity of the quinone in the PS I complex while the intercept ($1/f_a$) of the modified Stern-Volmer plot gives information on the accessibility of the quinone to excitations and on the quenching efficiency at the quinone binding site. The theory also predicts that if excitations are delocalized among all chlorophylls within the PS I complex, then the K_{SV} and f_a values determined from steady state fluorescence should be equal to those from P700 photooxidation measurements. We have applied this theory to isolated PS I complexes in order to evaluate the dynamics of excitation transfer among the PS I core antenna chlorophylls.

Tu-AM-A3

DIPOLAR ELECTRON SPIN-LATTICE RELAXATION OF RADICALS IN PROTEINS. INTERACTION OF THE STABLE TYROSINE RADICAL IN PHOTOSYTEM II WITH THE NON-HEME FE(II).

Donald J. Hirsh, Warren F. Beck, Jennifer B. Innes, and Gary W. Brudvig, Department of Chemistry, Yale University, 225 Prospect Street, New Haven, Connecticut 06511

The stable tyrosine radical $Y_D^\bullet$ (tyrosine-160 in the D2 polypeptide) in photosystem II (PSII) exhibits nonexponential electron spin-lattice relaxation transients at low temperature. Saturation-recovery relaxation transients of $Y_D^\bullet$ are compared with those of a model tyrosine radical, generated by UV photolysis of L-tyrosine in a borate glass, to determine the magnitude and mechanism of relaxation enhancement by paramagnetic sites in PSII. As previously reported, the polynuclear Mn complex in PSII that serves as the catalyst for photosynthetic water oxidation has a significant effect on the relaxation of $Y_D^\bullet$. However, the spin-lattice relaxation rate of $Y_D^\bullet$ in Mn-depleted PSII membranes is also enhanced by the high-spin non-heme Fe(II) and the relaxation transients are also nonexponential. We account for the nonexponential relaxation transients obtained from $Y_D^\bullet$ in Mn-depleted PSII membranes in terms of a dipolar relaxation mechanism with a powder distribution of relaxation rates. From simulations of the spin-lattice relaxation transients we obtain the magnitude of the magnetic dipolar interaction between $Y_D^\bullet$ and the non-heme Fe(II), which can be used to calculate the distance between them. Using data on the non-heme Fe(II) in the reaction center of *Rb. sphaeroides*, to model the non-heme Fe(II) in PSII, we calculate a $Y_D^\bullet$ - Fe(II) distance of ≥ 35 Å in PSII. This agrees well with the distance predicted from the structure of the bacterial reaction center.
[Work supported by NIH grant GM 36422.]

Tu-AM-A4

THE INFLUENCE OF ELECTRIC FIELDS ON PHOTOSYSTEM II FLUORESCENCE AND PRIMARY CHARGE SEPARATION

Holger Dau *, Robert Windecker #, Ulf-Peter Hansen #, Kenneth Sauer * (Intro. by Melvin Calvin)

* Laboratory of Chemical Biodynamics, Lawrence Berkeley Laboratory, California 94720, USA
# Institut fuer Angewandte Physik, Universitaet Kiel, Leibnizstr. 11, D-2300 Kiel, FRG

1. The influence of light-induced thylakoid voltages on the yield of chlorophyll fluorescence was studied on intact leaves of Aegopodium podagraria by comparing the fluorescence responses as induced by changes in light intensity to electrochromic absorbance changes. A linear kinetic analysis reveals that an increase in fluorescence yield by 5.4% originates from an increase in thylakoid voltage of only 10 mV.

2. A diffusion potential was set across the thylakoid membranes of spinach by salt jumps. This approach allows one to study the electric field dependence of Photosystem II fluorescence in more detail.

The results are discussed under the assumption that the electric field dependence of the fluorescence yield reflects the electric field dependence of the primary charge separation of Photosystem II.

Tu-AM-A5

UNIQUE ROLE(S) OF BICARBONATE IN PHOTOSYSTEM II REACTION CENTERS. Govindjee, Department of Physiology and Biophysics, University of Illinois, Urbana, Il 61801.
A working hypothesis for unique role(s) of HCO_3^-/CO_2 in photosystem II (PSII) of plants and cyanobacteria is now emerging. It appears that, at physiological pH, HCO_3^-/CO_2 may bind to certain amino acids on both D1 and D2, the reaction center proteins of PSII, and to iron between Q_A (bound to D2) and Q_B (bound to D1). HCO_3^-/CO_2 plays discrete and unique role(s) in PSII: its function may involve stabilization, by conformational means, of the reaction center protein that allows efficient electron flow in PSII, and efficient protonation of certain amino acids near Q_B^-. (See, e.g., Photosynthesis Research 19:85-128, 1988.) We shall review data on the differential sensitivity of mutants, altered in single amino acids, that support the involvement of both the D1 and the D2 proteins in the bicarbonate-reversible formate inhibition of PSII reactions. In D1 mutants of Synechocystis 6714, the resistance of cells to formate was in the following order (highest to lowest): A251V/F211S(AzV)>F211S (AzI) ≈ wild type> S264A (Govindjee et al., FEBS Lett 267:273-276, 1990a); in D1 mutants of Chlamydomonas reinhardtii, the order of resistance was: L275F(Br202)>A251V(Mz2)>> wild type ≈ F255Y(Ar207)≈ V219I(Dr18)>>S264A(DCMU4) (Govindjee et al., Photosynth Res, submitted, 1990b). In site-directed mutants of Synechocystis 6803, the order of resistance was: wild type>>R233Q ≈ R251S suggesting that these arginine residues may stabilize HCO_3^-/CO_2 binding (Cao et al., Abstract, Midwest Photosynthesis Conference, 1990). In contrast to plants and cyanobacteria, purple (Shopes, et al., Biochim.Biophys. Acta 974:114-118, 1989) and green (Govindjee, Trost and Blankenship, unpublished, 1990) photosynthetic bacteria, that contain Q_A and Q_B on their M and L subunits, respectively, donot show any bicarbonate-reversible formate effects. Possible reasons for differences between the systems examined and a possible role of HCO_3^-/CO_2 in protecting against photo-inhibition in PSII will also be discussed.

Tu-AM-A6

THE REACTION OF CYTOCHROME c_2 WITH PHOTOSYNTHETIC REACTION CENTERS FROM RHODOPSEUDOMONAS VIRIDIS.
David B. Knaff[1], Anne Willie[2], Joan E. Long[2], Aidas Kriauciunas[1], Bill Durham[2] and Francis Millett[2].
[1]Dept. of Chemistry & Biochemistry, Texas Tech University, Lubbock, TX; [2]Dept. of Chemistry & Biochemistry, University of Arkansas, Fayetteville, AR
The reactions of Rps. viridis cytochrome c_2 and equine cytochrome c with Rps. viridis reaction centers were studied using flash excitation. Single flash excitation of detergent-solubilized reaction centers resulted in rapid photooxidation of the cytochrome c-556 component of the reaction center. Photooxidized cytochrome c-556 was then reduced by cytochrome c_2 with a rate constant that exhibited a hyperbolic dependence on cytochrome c_2 concentration, suggesting formation of a complex between the cytochrome and the reaction center with K_d=30 μM. The rate of electron transfer within the complex was 270 s^{-1}. This reaction was not inhibited by oxidized cytochrome c_2. Addition of quinone to the depleted Q_B site of the reaction center allowed double flash experiments to be carried out. The double flash experiments indicated that cytochrome c_2 is not rapidly oxidized by photooxidized cytochrome c-559 of the reaction center and that the dissociation of photooxidized cytochrome c_2 from the reaction center is relatively rapid. The observed rate constant for cytochrome c_2 oxidation by photooxidized cytochrome c-556 decreased 14-fold as the ionic strength was increased from 5mm to 1M, suggesting that electrostatic interactions contribute to complex formation between the soluble cytochrome and the reaction center. Equine cytochrome c was also oxidized by photooxidized cytochrome c-556 but, despite the high sequence homology between it and cytochrome c_2, the reaction was much slower than with the Rps. viridis cytochrome and no evidence for complex formation with the reaction center was observed. Similar results were obtained using Rps. viridis membranes instead of detergent-solubilized reaction centers.
Supported by grants from N.S.F.(DCB-8806609 to D.B.K.), N.I.H.(GM20488 and RR07101 to F.M.) and the Welch Foundation (D-0710 to D.B.K.)

Tu-AM-A7

ELECTROSTATIC DESTABILIZATION OF THE CYTOCHROME b_6f COMPLEX IN THE THYLAKOID MEMBRANE. A. Szczepaniak and W.A. Cramer (Intro. by C. B. Post), Dept. of Biological Sciences, Purdue University, West Lafayette, IN 47907.

The three most hydrophobic large polypeptides of the chloroplast cytochrome b_6f complex were sequentially extruded from the membrane, in the order, cyt b_6, suIV, and Rieske iron sulfur protein, as the pH was increased in the alkaline region from 10 to 12, a protocol usually employed to remove extrinsic or peripheral proteins from membranes. The extruded proteins were non-membranous and not sedimented at 100,000 x g. The pH values for half-extrusion were approximately 10.7, 11.1, and 11.3, respectively. The most hydrophilic of the large b_6f polypeptides, cytochrome *f*, was not extruded. In addition to the loss from the membrane fraction of the immunoreactive polypeptide, the extrusion of cytochrome b_6 from the membrane was also reflected by the absence of its characteristic reduced minus oxidized absorbance signal. The pH values at which extrusion occurred increased as the ionic strength was raised. It was inferred that the pH-dependent extrusion of the three polypeptides of the cytochrome b_6f complex is caused by deprotonation of peripheral lysine and tyrosine residues, which results in a large increase in net negative charge, estimated to be -12, -11, and -10 for cyt b_6, suIV, and the FeS protein, and increased electrostatic repulsion between the peripheral polar segments of neighboring polypeptides and the membrane surface. The repulsion energy is sufficient to separate the polypeptides of the complex which are normally isolated together in detergent, and to cause their sequential extrusion from the membrane. This implies that electrostatic stabilization is important in the specific assembly of the cytochrome b_6f complex in the thylakoid membrane (supported by NIH GM-38323).

Tu-AM-A8

TRUNCATION ANALYSIS OF STRUCTURE-FUNCTION OF THE CYTOCHROME b_{559} α SUBUNIT IN THE PSII REACTION CENTER. G.-S. Tae and W. A. Cramer, Dept. of Biological Sciences, Purdue University, West Lafayette, IN 47907

The cytochrome b_{559} α subunit spans the bilayer once, with its NH_2- and COOH-termini oriented on the stromal and lumenal sides of the thylakoid membrane, respectively (1,2). The lumen- exposed COOH-terminal segment of 35-40 residues is shielded by the 33 kDa OEC polypeptide and at least one other polypeptide (3). The COOH-terminal segment was sequentially truncated in *Synechocystis* sp. PCC 6803 in order to determine the minimum length of the functional α subunit and its COOH-terminal domain.

Mutants with different lengths of the COOH-terminal domain were generated using site-directed mutagenesis by introducing a stop codon at R-51 (αR51), R-60 (αR60), and Y-70 (αY70) of the *psbE* gene and transforming mutated plasmids into *psbE*$^-$ T1297(4), kindly provided by H. Pakrasi, to generate 31-, 22-, and 12- residue truncated mutants. The mutants can grow photoautotrophically, the growth rate of αR51 and αR60 < wild type, and that of αY70 ≈ wild type. The O_2 evolving activity of αR51, αR60, and αY70, measured with cells, was 20%, 30%, and 80% of wild type, whereas the PSI activities of these mutants were similar to wild type.

The room temperature fluorescence yield (F_{max}) of the three mutants, measured in the presence of 20 μM DCMU, was 30%, 40%, and 90% of wild type for the αR51, αR60, and αY70 mutants. The addition of either 5 mM hydroquinone or 10 mM hydroxylamine did not increase the fluorescence yield of these mutants to the level of wild type, indicating that the low O_2 evolving activities of αR51 and αR60 may not be due only to OEC donor side malfunction. 77°K fluorescence emission spectra of the three mutants indicated that the emission peak at 696 nm, but not at 685 nm, is absent in αR51 and αR60, whereas αY70 has both peaks. Western blotting of the CP-47 polypeptide indicated that it exists in all three mutants. This implies that the PSII core complex of αR51 or αR60 is assembled in the thylakoid membrane, but the interaction between the PSII core and CP-47 is lost because of the 20-30 residue truncation of the cytochrome b_{559} α subunit (supported by NIH GM-38323).

(1) Cramer *et al.* (1986) *Photosynth. Res.* **10**, 393-403; (2) Tae *et al.* (1988) *Biochemistry* **27**, 9075-9080; (3) Tae *et al.* (1989) *FEBS Lett.* **259**, 161-164; (4) Pakrasi *et al.* (1988) *EMBO J.* **7**, 325-332.

Tu-AM-A9

CHARACTERIZATION OF RHODOBACTER SPHAEROIDES REACTION CENTER MUTANTS DESIGNED TO EXPLORE DIMER MIDPOINT POTENTIALS.

Heather A. Murchison, Neal W. Woodbury, Aileen K. Taguchi, James P. Allen, and JoAnn C. Williams. Center for the Study of Early Events in Photosynthesis, Department of Chemistry, Arizona State University, Tempe, AZ 85287-1604.

Several Rhodobacter (Rb.) sphaeroides mutants were designed to probe the involvement of the protein subunits of the reaction center (RC) in modulating the midpoint potential of the dimer (P). Woodbury et al. (1990) constructed a mutant Rb. capsulatus RC, pAT-3, which exhibits a P midpoint potential 200 mV higher than the potential of P in the wild type RCs. It was constructed by replacing an eighteen amino acid region of the M subunit with the symmetry related region from the L subunit. The equivalent changes are being made in Rb. sphaeroides and are shown in the table below. Four related single amino acid changes (see table) have been constructed in Rb. sphaeroides to determine the contribution of individual amino acids in the modulation of the P midpoint potential. The mutants are being made in Rb. sphaeroides so that both the structural and functional properties can be determined. RCs from all five mutants will be characterized using spectroscopic techniques such as visible and near IR absorption spectroscopy, fluorescence quenching, and subpicosecond transient absorption spectroscopy. P midpoint potentials for the mutant RCs will be determined and compared to the potentials for wild type Rb. sphaeroides and Rb. capsulatus pAT-3 RCs. These data will be presented, along with a progress report on the effort to determine the three dimensional structures of the mutant RCs by x-ray crystallography.

Table. Rb. sphaeroides mutants.

M subunit M188-M206	N F S L V H G N L F Y N P F H G L S I
L M196 to F M196	- - - - - - - - - - - - F - - - - - - - - - - - - -
F M197 to H M197	- - - - - - - - - - - - - H - - - - - - - - - - - -
L subunit L159-L177	N T G Y T Y G N F H Y N P A H M I A I
F L167 to L L167	- - - - - - - - - - - - L - - - - - - - - - - - -
H L168 to F L168	- - - - - - - - - - - - - F - - - - - - - - - - - -

Woodbury, et al. (1990) Proc. "Structure and Function of Bacterial Reaction Centers" Feldafing, ed. Michel-Beyerle, M., Springer-Verlag, Heidelberg.

Tu-AM-B1

ISOLATION AND CHARACTERIZATION OF AN INTEGRAL HEPARAN SULFATE PROTEOGLYCAN SYNTHESIZED UPON SUBSTRATUM-INDUCED OLIGODENDROCYTE DIFFERENTIATION. J.E. Sherin* and S. Szuchet, Dept. of Neurology & The Brain Research Institute, University of Chicago, Chicago, IL 60637.

In earlier work, we have shown that substratum-induced differentiation of oligodendrocytes (OLGs) signals the synthesis of peripheral proteoglycans (PGs) and sulfated glycoproteins (Gps) that segregate within the plasma membrane (PM) leading to cell polarization. We now report that OLG-substratum adhesion induces the synthesis of a high mol. wt. heparan sulfate proteoglycan (HSPG) that is an integral component of OLG PM. We speculate that this PG may be a receptor for peripheral PGs. Parallel OLG cultures that differed in 24h of adherence only were labeled with carrier-free $^{35}SO_4^{2-}$ for 24h. After washing off free label and removing peripheral PGs with 0.1 mg/ml of heparin, cell pellets were extracted with 1% Triton X-100 and insoluble pellets were re-extracted with 4M guanidine.HCl (Gu.HCl) + 0.1% Triton X-100. Supernatants containing solubilized material were fractionated on Sepharose CL-4B. The elution profiles revealed an increased amount of sulfated material in the attached OLGs (B3.fA) compared to the non-attached OLGs (B3.f). To assess if there are qualitative differences between B3.f and B3.fA OLGs, fractions were resolved by SDS-PAGE and detected by fluorography. The major component in the Triton-extract of B3.fA OLGs was a sulfated macromolecule (M_r≈100K); no PGs were detected. A band of the same M_r was seen in B3.f OLGs but at a much lower concentration. A $^{35}SO_4^{2-}$-labeled band M_r>200K was detected in the Gu.HCl extract of B3.fA but not in B3.f OLGs (at equal exposure time). Degradation by heparatinase but not by chondroitinase ABC proved that this component is a HSPG. To test whether or not extracted PGs/Gps might be receptors for peripheral PGs, we examined their ability to bind to heparin. OLGs were double labeled with [^{3}H]met and $^{35}SO_4^{2-}$ and extracted first with Triton followed by Gu.HCl. Each extract was fractionated on a heparin-affinity column using a linear gradient from 0.1M - 1.5M NaCl for elution. From the Triton-extract, only one sulfated Gp bound to this column at physiological ionic strength and was eluted between 0.36M to 0.6M NaCl. The elution profile of the Gu.HCl-extract was complex, consisting of a HSPG (0.25M - 0.4M NaCl) and 2-3 components weakly labeled with $^{35}SO_4^{2-}$ (0.4M - 1.0M NaCl). Whether or not one of these components is the receptor involved in signaling substratum-induced differentiation and/or binding of peripheral PGs is under investigation. Supported by grant NS PO1-24575-03.

Tu-AM-B2

HISTAMINE ACTS AT H_2-LIKE RECEPTORS TO INCREASE A CHLORIDE CONDUCTANCE IN MOTONEURONS OF THE CARDIAC GANGLION OF THE LOBSTER (*HOMARUS AMERICANUS*). Hossein Hashemzadeh-Gargari and Joseph E. Freschi (Intro. by John Pooler). Department of Neurology, Emory University, Atlanta, GA 30322.

In neurons from several arthropod and molluscan species, histamine acts directly to activate a chloride conductance. We studied the effect of histamine on the lobster cardiac ganglion, a simple network consisting of 4 small pacemaker neurons and 5 large motoneurons. Histamine inhibited the spontaneous rhythmic burst activity. In motoneurons under voltage clamp, histamine caused a dose-dependent current at doses between 1 and 100 μM. The H_2 antagonist cimetidine competitively inhibited the response at concentrations between 1 and 20 μM. The H_1 antagonists, cyproheptadine and chlorpheniramine, had only weak inhibitory effects at high concentrations (above 100 μM). With microelectodes filled with 3M KCl, the histamine-activated current was inward at membrane potentials held near the resting potential of -45 to -50 mV. The current reversed at -35 mV and became outward at more positive membrane potentials. With electrodes filled with 3M K^+ acetate, the histamine-evoked current reversed at -55 mV. When the extracellular [Cl^-] was reduced, the histamine current reversal potential shifted to more positive values as predicted by the Nernst equation for [Cl^-]. Altering extracellular [Ca^{2+}] or [Na^+] did not affect the histamine response. Current-voltage curves of the histamine-evoked current showed outward rectification, and measurement of the chord conductance as a function of membrane potential showed that the histamine-activated chloride conductance was voltage-dependent. Histamine appears to act like GABA in directly activating a Cl^- conductance to inhibit the patterned motor output from the cardiac ganglion. (Supported by NIH grant NS-22628).

Tu-AM-B3

EFFECTS OF PAVLOVIAN CONDITIONING ON *HERMISSENDA*'S B-PHOTORECEPTOR POTASSIUM CHANNELS. R. Etcheberrigaray, L. D. Matzel, I. I. Lederhendler and D. L. Alkon. Laboratory of Molecular and Cellular Neurobiology, NINDS, National Institutes of Health, Bethesda, Maryland 20892.

Pavlovian conditioning induces reduction of two potassium currents (I_A & I_C) across the soma membrane of the type B photoreceptor of *Hermissenda crassicornis* . This effect can be mimicked by activating protein kinase C (PKC). At the single channel level, we have described a 42 pS (*medium*) and a 64 pS (*large*) K^+-channel. We have also found that the PKC activator phorbol-12-13-dibutyrate, reduces the open probability of the large channel. In the present study, we used the patch-clamp technique to study single K^+-channels 24 hours after conditioning. Acutely isolated eyes were obtained from naive, unpaired or conditioned animals. Cell-attached experiments revealed that the large channel was seen in 20% of the patches from conditioned animals (n=10), compared to 59% in naive (n=27) and 50% in unpaired animals (n=6), Chi-sq.=4.52, p< 0.05. When this channel was present, its percentage of open time in conditioned animals was about 45% reduced compared to naive (35.71±2.94, n=7) and unpaired animals (33.12±3.71, n=6). The medium channel was present with the same frequency in all three groups (about 80% of the patches). The percentage of open time of the *medium* channel was slightly reduced in conditioned (6.85±3.58, n=8) compared to naive animals (12.17±3.8, n=11). These results indicate that Pavlovian conditioning has a major effect (similar to PKC activation) on the *large* (64 pS) channel.

Tu-AM-B4

INOSITOL TRISPHOSPHATE PROMOTES I_{Na-Ca} BY RELEASING CALCIUM FROM SARCOPLASMIC RETICULUM IN CARDIAC MYOCYTES. James C. Gilbert and Achilles J. Pappano (Intro. by Dr. Bruce Koeppen) Department of Pharmacology, University of Connecticut Health Center, Farmington, CT 06030.

Membrane depolarization sufficient to activate sodium but not calcium current evoked an early inward tail current in voltage-clamped ventricular myocytes. This early inward tail current required Na_o and Ca_i and is thought to follow earlier reverse mode Na-Ca exchange that triggers Ca^{2+} release from sarcoplasmic reticulum (SR). Inhibitors (ryanodine, caffeine) and promoters (intracellularly dialyzed IP_3) of SR Ca^{2+} release decreased and increased, respectively, the magnitude of the early inward tail current.

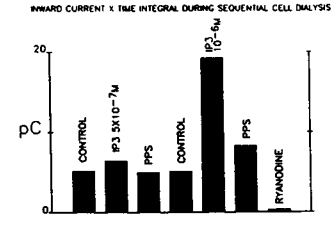

Legend: inward current x time integrals upon stepping from -80 to -40mV during sequential dialysis: control solution; IP_3, 500nM; pentosan polysulfate (100μg/ml, PPS), an IP_3 inhibitor; control; IP_3, 1μM; PPS. Last column shows superfusion with ryanodine (1μM) containing Tyrode's solution.

The results substantiate the hypothesis that Ca^{2+} release from the SR participates in early I_{Na-Ca} and show that IP_3, by releasing Ca^{2+} from the SR, can promote Na-Ca exchange across the plasma membrane.

Tu-AM-B5

LOCALIZATION OF ODOR TRANSDUCTION IN ISOLATED OLFACTORY RECEPTOR CELLS.

Graeme Lowe and Geoffrey H. Gold,
Monell Chemical Senses Center, Philadelphia, PA 19104.

We have studied the spatial distribution of odorant sensitivity and odorant-induced currents in dissociated tiger salamander olfactory receptor cells. Simultaneous suction electrode and whole-cell recording showed that odorant stimulation causes an inward generator current in the cilia. The resulting membrane depolarization activates an outward current (amplitude < 100 pA) through somatic voltage-dependent conductances.

The odorant sensitive region of the cell was mapped by recording the outward somatic current with a suction electrode, while stimulating locally by pressure ejecting an odorant solution from a nearby micropipette. Continuous flow of Ringer's solution (500 μm/s) was used to align the cilia and dendrite along a single axis, and to limit the region of the cell exposed to the stimulus. Starting at the tips of the cilia, response amplitude increased approximately linearly with the length of cilia exposed to the stimulus, reaching a maximum at the bases of the cilia. Thus, odorant sensitivity is confined to the ciliary region. Sensitivity is uniform along the length of the cilia, indicating that all components of the transduction mechanism are uniformly distributed throughout the cilia and that the cilia are electrotonically compact. Responses to high K+ in the stimulus solution showed that the resting K+ conductance was lower in the cilia than in the dendrite and cell body. This lower density of K+ channels may serve to maximize the electrotonic length of the cilia. Varying the stimulus position did not affect the latency (variation less than 50 ms) or the time course of the odor response. Thus, transduction is local, and does not require the diffusion of odorants or intracellular messengers from the cilia to the dendrite (diffusion time ca. 250-400 ms).

Our results indicate that all components of the transduction mechanism, from the odorant receptors to the channels which carry the generator current, are localized to the cilia.

Supported by NIH Grant DC00505.

Tu-AM-B6

IONTOPHORETIC APPLICATION OF CHANNEL BLOCKERS LOCALIZES MECHANOELECTRICAL TRANSDUCTION TO THE HAIR BUNDLE'S TIP.

F. Jaramillo and A. J. Hudspeth, Department of Cell Biology and Neuroscience, Southwestern Medical Center, Dallas, Texas 75235.

Stimulation of a hair bundle, the receptive organelle of a hair cell, controls the opening and closing of mechanically sensitive ion channels. To understand how these channels are gated, it is essential to determine where they are located with respect to the bundle's constituent stereocilia. Focal extracellular recordings of potentials around stimulated hair bundles indicated that transduction channels reside near the distal tips of the stereocilia (Hudspeth, A. J., *J. Neurosci.* **2**: 1-10 [1982]). Attempts to localize the channels by measuring Ca^{2+} influx through them gave contradictory results. Measurements using the indicator fura-2 suggested an increase in Ca^{2+} concentration near the bases of stimulated hair bundles, where transduction was accordingly believed to occur (Ohmori, H., *J. Physiol.* **399**: 115-137 [1988]). When the Ca^{2+} influx through transduction channels open at rest was detected with the indicator fluo-3, maximal fluorescence was instead observed near the stereociliary tips, a result consistent with the channels' being situated there (Huang, P. L. and Corey, D. P., *Biophys. J.* **57**: 530a [1990]).

We have attempted to identify the site of mechanical sensitivity by focally inactivating transduction with aminoglycoside antibiotics, which are reversible channel blockers. Hair cells were enzymatically isolated from the bullfrog's sacculus and attached to a glass coverslip so that their bundles could be viewed in profile. Responses to mechanical stimuli were recorded with the perforated-patch variant of the whole-cell recording technique. While a transduction current was elicited by protracted hair-bundle deflection, dihydrostreptomycin or gentamicin was iontophoretically applied from an electrode situated 1-2 μm above a hair bundle's side. The local sensitivity of transduction to the blocker was then sampled by moving the iontophoretic electrode to 64-256 different locations in a grid centered upon the bundle.

Aminoglycoside antibiotics reduced transduction currents only when applied near the tips of hair bundles. Iontophoretic ejections were consistently most effective when directed precisely at the stereociliary tips, but had no effect when administered at the bases of stereocilia or at cuticular plates. Our results support the hypothesis that the mechanoelectrical-transduction channels of hair cells are located near the stereociliary tips.

This research was supported by National Institutes of Health grant DC00317.

Tu-AM-B7

CHEMORECEPTIVE CAPABILITIES OF THE SQUID OLFACTORY ORGAN.

M.T. Lucero, F.T. Horrigan, J.L. Levitt, and W.F. Gilly. Hopkins Marine Station of Stanford University, Pacific Grove, CA 93950.

We have examined the effects of chemical stimuli on the so-called olfactory organ of the squid Loligo opalescens. Chemosensory responses were tested with behavioral assays on living squid and with whole-cell voltage clamp and 'perforated patch' current clamp techniques on the isolated receptor cells. Low concentrations of certain test substances reproducibly elicited escape responses in living, restrained squid. We mapped the region of highest chemosensitivity directly to the olfactory organ which is a small knob composed of neuronal and ciliated epithelial cells located in an ear-like flap lateral to each eye. 'Ablation' experiments, performed by treating the olfactory organ with a local anesthetic, further confirm the olfactory organ as a site of chemoreception. In examining isolated chemosensory cells, we observed at least three morphologies, similar to those described by Emery (1975) in ultrastructural studies. Voltage clamp experiments on the two most common cell types (pyriform and floriform) indicate that they contain voltage-gated Na^+, K^+ and Ca^{+2} channels. The same cells under current clamp are capable of generating spontaneous and repetitive action potentials that are blocked by TTX. K^+ channel blockers such as 4-amino-pyridine, TEA, and TBA, or blockers of both Na^+ and K^+ channels (methadone and propyl paraben) reliably elicit escape responses when applied to the squid olfactory organ. Natural products such as squid ink, fish mucus, or a snail hypobranchial gland extract also elicit strong escape jetting responses.

Tu-AM-B8

The relationship between extracellular pH (pH_o) and intracellular pH (pH_i) in adult rat carotid body glomus cells. T.J. Wilding, B. Cheng, and A. Roos. Department of Cell Biology and Physiology, Washington Univ. Sch. of Med., St. Louis, MO 63110.

In our in-vivo carotid body studies, some 30 years ago, we assigned a "pre-eminent" role to arterial pH, i.e., pH_o, rather than to pCO_2 or $[HCO_3^-]_o$ by themselves as a chemoreceptor stimulus. Since pH_i may play a role in the response of the carotid body to pH_o, we have studied the pH_o-pH_i relationship at 36°C in single glomus cells loaded with the pH-sensitive fluorescent dye BCECF. In HEPES- or PIPES-buffered media, pH_i strikingly responded to pH_o (6.2-8.0): $pH_i = 2.86 + 0.57\ pH_o$ (n=17; corr. coef. 0.9). As in other cells, intrinsic buffering power, β, measured with small pulses of NH_4Cl, increased with decreasing pH_i: $\beta = 84.9 - 9.8\ pH_i$ (n=22; corr. coef. 0.8). The pH_i response to Na removal (substitution by NMDG, pH_o 7.4) was also marked: pH_i fell from an average of 7.30 (140 Na) to 6.38 (0 Na) (n=8) in ~15 min. Average pH_i at intermediate Na concentrations (50 and 20) was 7.07 (4) and 6.87 (9), resp. When, at 50 Na, 15 μM hexamethylene amiloride (HMA), a powerful Na/H exchange inhibitor, was added to the superfusate, pH_i fell. The fall was, however, somewhat less than was observed in the same cell upon Na removal. HMA also greatly reduced recovery from NH_4Cl-prepulse acidification (pH_o 7.4; 20 Na).

In CO_2/HCO_3^- buffer, reducing pH_o by ~0.6 either by lowering HCO_3^- from 25 to 5 (5% CO_2) or by raising pCO_2 from 1 to 5% (5 HCO_3^-) reduced pH_i by 0.3-0.6. The same external acidification in HEPES and in CO_2/HCO_3^- had nearly the same effect on pH_i. Simultaneously raising pCO_2 (from 1% to 5 or 10%) and HCO_3^- at unchanged pH_o of 7.4 produced a transient acidification, but had little effect on steady-state pH_i. Changing the superfusate's buffer from HEPES to 5 or 10% CO_2-HCO_3^- (pH_o always 7.4) similarly did not produce much of a steady state pH_i change. The unusual sensitivity of pH_i to pH_o suggests that the intracellular pH of the glomus cell may be a link in the chemoreceptor's response to changes in external acidity. (Supported by NIH Grant 00082).

Tu-AM-B9

NONLINEAR ANALYSIS OF SENSORY ENCODING IN A RAPIDLY ADAPTING INSECT MECHANORECEPTOR.

A.S. French and L.L. Stockbridge, Department of Physiology, University of Alberta, Edmonton, Alberta T6G 2H7, Canada.

The cockroach femoral tactile spine contains a single neuron whose activity adapts rapidly and completely to step deformations. This rapid adaptation occurs during action potential encoding from the receptor current and has two separable components. Nonlinear systems analysis of encoding in the tactile spine has previously been carried out by random extracellular stimulation followed by Wiener kernel estimation. The resulting nonlinear description was well-fitted by a model consisting of a cascade of linear dynamic, nonlinear static, and linear dynamic components, where the static nonlinearity had the form of a half-wave rectifier and was believed to reflect the voltage activation of a regenerative sodium current. However, firm associations between the components of the nonlinear model and cellular functions are not yet possible.

We have recently developed a technique for reliable intracellular recording from the region of the sensory neuron where action potential encoding occurs. Nonlinear systems analysis was performed on this preparation by injecting a pseudo-random current (0-500 Hz bandwidth) to cause continuous firing of action potentials. The resultant fluctuations in membrane potential were recorded, together with action potentials, which were typically less than 1 ms duration. A computer algorithm separated the recording into input (membrane potential) and output (action potentials) prior to computation of Wiener kernels, using both cross-correlation and orthogonal estimation techniques.

The static nonlinear component was again a half-wave rectifier and the first-order kernel had high-pass form. However, the cascade model had significant differences from previous estimates with implications for the mechanism of rapid adaptation.

Supported by the Canadian Medical Research Council.

Tu-AM-B10

BRAIN WAVES--ART OR ARTIFACT: CARDIAC PERIODICITY AND SUPPORT FOR A NON-NEURAL ELECTROMECHANICAL ORIGIN HYPOTHESIS

Horace Castillo
Rogers Heart Foundation, St. Anthony's Hospital
St. Petersburg, Florida U.S.A.

Dan Sapoznikov
Dept. Cardiology, Hadassah Univ. Hospital
Jerusalem Israel

The origin of EEG has been obscure since its introduction by Berger in 1929. A summation of neural discharges has generally been accepted as the source of potential and modulation. However, theory, models, lab and clinical experience suggest that a non-neural electromechanical origin can be supported. DC standing potentials from electrodes, membrane, liquid junctions and static charges may be mechanically modulated by the arterial pulse. Instrumentation band limits the signal (1-70 Hz) removing neural spikes and differential amplification may contribute to the "beat" pattern of Alpha. Signal averaging with ECG QRS trigger and "eyes open" gives a pattern of cardiac periodicity. It was previously observed that eye muscle tremor during "eyes closed" obscured cardiac periodicity. Naturally the ECG and arterial pulse are recovered with signal averaging. However, the first third of the cycle has greater randomness than the last two-thirds. There has been recovery from electrical brain death. An electromechanical origin for EEG may assist with understanding this clinical observation.

Tu-AM-C1

DEPENDENCE ON THE INITIAL FORCE OF APPARENT EFFICIENCY OF THE ATP-INDUCED ACTIN-MYOSIN SLIDING IN PRODUCING WORK STUDIED USING AN *IN VITRO* FORCE MOVEMENT ASSAY SYSTEM.

H. Sugi, K. Oiwa and S. Chaen. Department of Physiology, School of Medicine, Teikyo University, Itabashi-ku, Tokyo 173, Japan.

To eliminate the gap between muscle physiology and biochemistry, we measured the amount of work done by the ATP-induced actin-myosin sliding using an *in vitro* force-movement assay system developed in our laboratory (Chaen *et al.* Proc. Natl. Acad. Sci. USA 86: 1510-1514, 1989). The assay system consists of a glass microneedle coated with rabbit skeletal muscle myosin and well-organized actin filament arrays (actin cables) in the giant internodal cell of an alga (*Nitellopsis obtusa*). The needle was made rigid, so that the distance of sliding of the myosin-coated needle tip was limited to about 1μm. The actin-myosin sliding was initiated by iontophoretic application of ATP, the ATP electrode being placed at 50μm distant from the needle tip. The amount of work done by the ATP-induced actin-myosin sliding was calculated from the needle movement recorded with a couple of phtodiodes.

By applying a constant amount of ATP with the same time course, it was found that the amount of work done by the actin-myosin sliding in response to a constant amount of ATP increased with increasing initial baseline force from zero to $0.5\text{-}0.6P_0$. These results seem to be analogous to the basic characteristics of contacting muscle. In the above range of initial baseline force, the velocity of the main part of needle movement was almost the same. The range of P_0 observed (500-1,000pN) indicated that the number of myosin molecules involved in the work production may be very small (250-500). As such a small number of myosin molecules may be activated to interact with actin cables almost simultaneously in response to the iontophoretically delivered ATP, the present results may be taken to imply that the force-velocity and the force-energy relations in muscle might reflect the basic properties of each myosin molecule rather than the change in number of myosin molecules involved in the work production.

Tu-AM-C2

VELOCITIES OF ACTIN FILAMENTS OCCUR IN DISCRETE POPULATIONS WHEN OBSERVED IN AN *IN VITRO* MYOSIN MOTILITY ASSAY.

Taro Q. P. Uyeda, Hans M. Warrick, Steve J. Kron and James A. Spudich. Department of Cell Biology and Developmental Biology, Stanford University School of Medicine, Stanford, CA 94305.

Fluorescently labeled actin filaments were observed in an *in vitro* motility assay using a low density (≈25/μm^2) of HMM molecules prepared from rabbit muscle, ATP and 1.75% methylcellulose at 30° C. The methylcellulose was required to reduce the lateral diffusion of the actin filament when unbound or weakly bound to low numbers of myosins. The average velocity of sliding observed was lower than for higher concentrations of HMM. The progress of the filaments could be interpreted as a combination of intervals of "runs" of directed movement and "pauses" containing random Brownian movements. The position of filaments were determined in successive video frames while they were undergoing directed movements. When a large number of observations were pooled, specific velocities occurred more frequently than would be expected in a random distribution. The peaks appeared to be regularly spaced and could be enhanced by applying filters which reduce random events in the data set. The spacing of the peaks did not change with different objectives (63X or 100X) but did change slightly (≈30%) with different preparations of HMM. The presence of peaks in the velocity distribution could be interpreted as the result of differences in the number of motors per actin filament. The minimum observed velocity would reflect the activity of a single HMM molecule, which when combined with the ATPase cycle time yields a step of <20 nm per ATP hydrolyzed. This distance is within the geometrical limits suggested by a tightly coupled swinging cross-bridge model of myosin action.

Tu-AM-C3

WHAT IS THE RATE LIMITING STEP FOR ACTIN FILAMENT MOVEMENT BY SMOOTH MUSCLE MYOSIN?

D. Warshaw and K. Trybus*, Univ. of Vermont, Physiol. & Biophys., Burlington, VT; *Rosenstiel Research Ctr, Brandeis Univ., Waltham, MA

Smooth muscle actomyosin interactions have been studied using an in vitro motility assay, in which fluorescently labeled actin filaments were observed moving over myosin adhered to a glass coverslip (Warshaw et al., J. Cell Biol. 111:453, 1990). To determine the rate limiting step for actin filament motion by thiophosphorylated smooth muscle myosin, the effect of changing MgATP, MgADP, and Pi concentrations on actin filament velocity was investigated. Changes in [MgATP] were accomplished by flash photolysis of "caged" ATP. At released [MgATP] > 0.7mM, actin filaments moved at their maximum velocity 30ms after the flash. These data suggest that nucleotide binding to the rigor complex, crossbridge detachment, hydrolysis, and reattachment do not limit actin filament velocity. However, at released [MgATP] < 0.1mM, actin filaments accelerated to their steady state velocity. The acceleration is presumably due to a decreased load with time caused by a declining number of rigor crossbridges at these low [MgATP]. The rate of acceleration varied between 0.6-3.0s^{-1} depending on [MgATP] and may reflect the rate of crossbridge cycling. This estimate of cycling rate is in the range of actomyosin ATPase rates obtained in solution. The flash photolysis experiments suggest that either Pi or MgADP release may be rate limiting. In experiments where [Pi] was increased to 24mM, no effect was observed on actin filament velocity. However, a pronounced reduction in actin filament velocity was observed in the presence of 2mM free MgADP. Analysis of these data showed that MgADP competes for the nucleotide binding site on myosin with a Ki=0.2mM. The reduction in actin filament velocity suggests that increasing [MgADP] results in a long-lived actomyosin-MgADP complex. Release of MgADP may be the rate limiting step for actin filament motion caused by thiophosphorylated smooth muscle crossbridges. (Support:HL45161(DW);HL38113(KT))

Tu-AM-C4

CARDIAC MUSCLE CROSSBRIDGE MECHANICAL INTERACTIONS DETERMINE ACTIN FILAMENT VELOCITY IN VITRO.

D. Warshaw, J. Peterson, and N. Alpert. Univ. of Vermont, Physiol. & Biophys., Burlington, VT 05405

Alterations in hypertrophied cardiac muscle mechanics may be related to the proportion of V1 and V3 myosin isoforms expressed within a muscle fiber. From previous studies, we proposed that V3 myosin cycles slower and spends a greater fraction of its cycle in a high force state (i.e. increased duty cycle) compared to the V1 isoform. To directly test this hypothesis, we used an in vitro motility assay in which fluorescently labeled actin filaments were observed sliding over mixtures of V1 and V3 myosin monomers adhered to a glass coverslip. V1 cardiac myosin was prepared from thyroxin-treated rabbits, whereas V3 myosin was obtained from pressure overloaded rabbit hearts. Using V3 myosin, actin filament velocity (1um/s) was 1/3 that observed with V1 myosin, which correlated with differences observed in both Ca^{+2}- and actin-activated myosin ATPases. When actin filaments interacted with mixtures of V1 and V3 myosins, actin velocity was graded with the V3 myosin predominating. The modulation of actin velocity may reflect a mechanical interaction between the two isoforms. We have developed a quantitative crossbridge mechanical interaction model (Warshaw et al., J. Cell Biol. 111:453, 1990) for the motility assay based on the force:velocity (F:V) relations of the muscles from which the myosin was isolated. To test the model's predictive capabilities, F:V were obtained from thyroxin-treated and pressure overloaded rabbit papillary muscles to constrain the model parameters. The motility data suggest that V3 myosin cycles slower and has a greater duty cycle than the V1 isoform. In addition, when using myosin mixtures, the prime determinant of velocity modulation is associated with the myosin having the greater duty cycle. This may have profound implications for cardiac muscle power, economy, and efficiency. (Support:HL45161(DW);HL07647(JP);HL28001(NA))

Tu-AM-C5

MOVEMENT OF ACTIN FILAMENTS BY PURIFIED MOLLUSCAN MYOSIN AND NATIVE THICK FILAMENTS

J.R. Sellers*, Y.J.Han* and B.Kachar+, NHLBI* and NIDCD+, Bethesda, MD 20892

We have shown that native thick filaments isolated from the adductor muscle of the clam *Mercenaria mercenaria* moves actin filaments both toward and away from the center of the thick filaments. Movement toward the center is ten fold faster than the rate of movement away from the center. We have extended this observation to several other molluscan thick filament preparations. Native thick filaments from the catch muscle of *Mercenaria* are 30-50 um in length. Actin filaments move toward the center of the thick filament at rates of 3.5 um/s and away the center at 0.35 um/s. Native thick filaments from the adductor muscle of the clam *Mya orenaria* move at 3.8 and 0.4 um/s while those from the ABRM muscle of *Mytillus edillus* move at 1.4 and 0.14 um/s respectively depending on direction of travel. Purified myosin from the adductor muscle of *Mercenaria* moves actin at a rate 6 um/s while that from the catch muscle moves at 2.7 um/s. These values are close to that reported for the fast speed on the native thick filaments. Movement of actin by *Mercenaria* adductor native thick filaments is dependent on calcium concentration. When pCa > 6 there is little or no movement and when pCa < 6 above actin filaments move at maximal or near maximal velocity. Few filaments move at intermediate velocities. When pCa > 6 few actin filaments bind to the thick filaments.

Tu-AM-C6

THE EFFECT OF REVERSIBLE REMOVAL OF LC1 ON CARDIAC Mg.S1.

S.S. Margossian*, H.D. White+, W.F. Stafford§, A. Malhotra+ and H.S. Slayter#. *Montefiore Med. Ctr. and §Albert Einstein Col. Med., Bronx, N.Y., +Eastern Virginia Med. Sch., Norfolk, Va., #Boston Biomed. Res. Inst., and #Dana-Farber Cancer Inst. and Harvard Med. Sch., Boston, Ma.

The reversible removal of the essential light chain, LC1, from dog cardiac Mg.S1 has made it possible to investigate the influence of LC1 on myosin subfragment 1 (S1) structure and activity. Upon analysis of dog heart Mg.S1 by SDS-PAGE, it became apparent that the essential light chain, LC1, had undergone substantial proteolysis. The presence of a 22-24kD band in Mg.S1 suggested that it could correspond to a partially cleaved LC1, but gel immunoblots with anti-LC1 and radioimmunoassays indicated that the 22-24kD band did not arise from LC1 and that more than 95% of the light chain had been removed. To recombine isolated LC1 with S1, 10-15 molar excess of the light chains and LC1-deficient Mg.S1 were mixed in the presence of ATP, Mg^{2+} and NH_4Cl, stirred for 20 min in the cold, followed by removal of excess light chains ion-exchange and gel exclusion chromatography. The resulting LC1-recombined S1, contained both LC2 and LC1 in a relative molar ratio of 1/1.3 with the 22-24kD fragment dissociated. Sedimentation equilibrium analysis revealed that LC1-recombined Mg.S1 behaved as a single monodisperse species with all three different molecular weight averages (M_w, M_n, M_z) superimposing and remaining constant at a value of 130±5kD over a concentration range of 0 to 1.5 mg/ml. Steady state rates of acto-S1 ATP hydrolysis were measured for the LC1-deficient and recombined Mg.S1. The V_{max} and K_c for LC1-deficient S1 were 0.4 s^{-1} and 30 μM respectively; the corresponding values after LC1 recombination were 0.8 s^{-1} and 7.5 μM. The K_{app}'s in the presence of ATP were 28 and 12 μM respectively for LC1-deficient and recombined Mg.S1. Moreover, Ca^{2+}-regulation was suppressed by anti-LC1 as evidenced by the total inhibition of the dog heart myofibrillar calcium-activated MgATPase. These results reveal that LC1 plays a significant role in the structure and function of cardiac myosin.

Tu-AM-C7

BACTERIALLY-EXPRESSED MAMMALIAN MYOSIN HEAD FRAGMENTS BIND LIGHT CHAIN 1 AND HAVE ENZYMATIC ACTIVITY

A.S. Rovner, M. Bravo-Zehnder, A.J. Straceski, E.M. McNally, and L.A. Leinwand, Department of M&I, F-416, Albert Einstein College of Medicine, Bronx, NY 10461.

Bacterial expression of rat cardiac myosin is being used to identify functional domains and to determine whether truncated myosin fragments synthesized *de novo* can attain the native conformation characteristic of their proteolytically derived counterparts. Myosin has 1 pair of heavy chains (MHCs), 2 pairs of light chains (MLCs), and can be segregated structurally into a carboxyl-terminal coiled-coil and two amino terminal globular heads (subfragment-1; S1). To identify the MHC sequences necessary for association with MLC1, we have co-expressed serially truncated segments of the MHCs with the full length ventricular MLC1. Immunological methods and subsequent SDS-PAGE showed that MHC and MLC1 associated with 1:1 stoichiometry in construct D1/MLC1, which expresses MHC aa 1-808 and is essentially identical to S1 produced by chymotryptic digestion of purified skeletal myosin (Maita et al., PNAS 84, 416-420). Construct D0/MLC1, containing a MHC of 790 aa, did not associate with MLC1, suggesting that aa 790-808 are necessary for MHC-MLC1 interaction. Preliminary studies have demonstrated both K^+/EDTA and Ca^{+2}-activated ATPase in crude extracts of D1/MLC1, but these activities are labile to further purification. Upon analysis by high-speed centrifugation, less than 35% of construct D2/MLC1 (encoding the amino-terminal 832 aa of the MHC) was soluble, while the D1/MLC1 construct containing MHC aa 1-808 was twice as soluble. Examination of the carboxyl-terminal 24 aa of D2/MLC1 revealed that this sequence is hydrophobic and highly conserved. Previous work (Mitchell et al., J. Mol. Biol. 208, 199-205) has suggested that this region of the MHC is necessary for MLC2 binding. Therefore, we propose that the lesser solubility of the D2/MLC1 product is due to its intermolecular aggregation via this "sticky tail", which is exposed in the absence of MLC2. We are currently testing this hypothesis using a triple construct which co-expresses the 832 aa MHC fragment, full-length MLC1, and MLC2.

Tu-AM-C8

DO VARIANT RESIDUES AMONG THE SIX ACTIN ISOFORMS OF DROSOPHILA REFLECT FUNCTIONAL SPECIALIZATION?

Mary C. Reedy*, Cliff Beall@ and Eric Fyrberg@. *Cell Biology, Duke University, Durham, N.C. @ Biology, Johns Hopkins, Baltimore, Md.

It is not known whether the ~27 amino acids which vary among the six actin isoforms of *Drosophila* confer differing functional properties or whether the variation reflects neutral drift accompanying separate regulatory control of the six actin genes in *Drosophila*. We have combined EM-analysis and site-directed mutagenesis of the flight-muscle-specific actin gene to probe the dependence of myofibril and crossbridge structure and function on variation of one or more of the variable residues (Table 1). We interconverted residues characteristic of actin which is functional in another cellular environment because mutations of highly-conserved residues are usually so disruptive as to preclude detailed analysis. The structure and function of the highly-ordered flight muscle (IFM) appear unaffected by most substitutions, indicating that interconversion of a single amino acid residue between isoforms is usually not sufficient to confer distinct function. However, introduction of several isoform-specific amino acid substitutions in combination does show effects *in vivo*. Using chimeric genes, many residues in the IFM actin gene were converted to those of larval, adult skeletal or cytoplasmic actin, thereby altering IFM sarcomere assembly. Substitution of the entire cytoplasmic sequence into the IFM indicates that the cytoplasmic actin isoform is not functionally and structurally equivalent to the IFM actin isoform.

Table 1

Mutation	Isoform specificity	Location	Effects
asp4>glu	leg,larval,cytoplasmic	myosin binding site	no
gly6>ala	larval, cytoplasmic	" " "	yes
ile 10>val	leg,larval,cytoplasmic	" " "	no
ile76>val	cytoplasmic	small domain 1	yes
ser129>thr	cytoplasmic	" "	no
thr234>ser	"	large domain 4	no
val278>thr	"	" " 3	no
gln360>glu	larval	myosin binding site	no
gly368>ser	cytoplasmic	" " "	no
chimeras:			
phe169>tyr, ala260>ser	larval		yes
" " ",cys257>thr	adult skeletal		no
ile76>val,ser129>thr,phe169>tyr,ala232>ser,thr234>ser,ala260>ser, ser271>ala,ile274>leu,val278>thr:	cytoplasmic		yes

Tu-AM-D1

STRUCTURAL STUDIES OF PROTEINS BY SOLID-STATE NMR

L.E. Chirlian* and S.J. Opella

Department of Chemistry, University of Pennsylvania, Philadelphia, PA 19104

Recent progress in the development of a general method for protein structure determination by solid-state NMR spectroscopy will be described. Measurements on membrane bound proteins and viral coat proteins are presented to demonstrate the utility of this method. Computational procedures are described to determine structure from these experimental results.

In this method, NMR measurements on nuclei of the planar peptide bond (peptide plane) provide limitations on the orientation of an individual peptide plane to within a few symmetry related possibilities. The peptide plane orientations can yield the structures of proteins that can not be crystallized and do not reorient rapidly enough for solution NMR experiments.

Tu-AM-D2

Phosphophoryn, a Mineral Matrix Ca^{2+}-Binding Protein. Evidence for the Presence of Anionic Cluster Domains in Phosphophoryn Which Possess Heterogeneous Secondary and Tertiary Structure.

John Spencer Evans and Sunney I. Chan, Laboratory for Chemical Physics, Division of Chemistry, California Institute of Technology,Pasadena California 91125

Bovine Dentine Phosphophoryn (BDPP) belongs to a class of proteins known as polyelectrolyte mineral matrix proteins (PMMP), which bind divalent cations and catalyze or regulate the formation of an inorganic mineral phase. Several approaches have bee adopted to study the structure of this unique protein. $^{1}H/^{31}P$ one- and two-dimensional NMR experiments have demonstrated that BDPP possesses anionic cluster domains comprised of repeat motifs of $(Asp)_n$, $(Pser)_n$, and $(Pser\text{-}Asp)_n$. Using K^+ as a probe for ion binding regions, we have demonstrated that at low molar ratios to BDPP (1:27) at pH 8.26, K^+ selectively binds to Pser residues located in domains which have the greatest negative charge density [i.e., $(Pser\text{-}Pser)_n$], but do not bind to Asp sidechains. At higher K^+:BDPP ratios (1:1, 3:1, 11:1), the remaining Pser and Asp become saturated. Using Monte-Carlo simulations (torquey-dynamics) and DREIDING I force-field, we have modeled N-terminal acetylated/C-terminal methyl ester peptides of $(Asp)_{10}$, $(Asp)_{20}$, $(Pser)_{10}$, $(Pser)_{20}$, $(Pser\text{-}Asp)_5$, and $(Pser\text{-}Asp)_{10}$ in the presence of saturating Na+. The resulting peptide structures which were generated demonstrated energetically favorable sequence-dependent secondary structures: $(Asp)_n$ peptides adopt conformations that are comprised of successive turns (Φ, Ψ = 30 to 100°); $(Pser)_n$ peptides adopt conformations which are comprised of repeats of turn regions followed by a short sequence (2 to 3 residues) that assumes an extended structure ($\Phi, \Psi > 120°$); and $(Pser\text{-}Asp)_n$ peptides adopt conformations which are best described as a repeat of a short turn motif (2 to 3 residues) followed by an extended region of 3 to 5 residues. These results support the concept of PMMPs as proteins that possess complex tertiary structures which permit the selective coodination of divalent cations to certain domains.

Tu-AM-D3

MULTINUCLEAR NMR STUDIES OF DIHYDROFOLATE REDUCTASE

T.-h Huang, F.Y. Huang, Q.X. Yang, L.E. Khaw, & #L. Gelbaum
School of Physics, *Biology, & #Research Center for Biotechnology, Georgia Institute of Technology, Atlanta, GA 30332.

Multinuclear NMR techniques were employed to study the structure and dynamics of E. coli dihydrofolate reductase (ECDHFR) in solution and in solid. The deuterium NMR spectra of lyophilized powder of (3',4'-D_6) trimethoprim (TMP) and (2',6'-D_2)TMP bound to DHFR detected no large amplitude (>15°) motion of rate > 10^4 S^{-1}. Hydrating the protein binary complex to 30 wt% resulted in a substantial spectral changes. Lineshape simulation showed that the methoxyl groups is exerting a rapid, large amplitude librational motion at a rate of 10^5 S^{-1}. In contrast, the benzyl ring appears to be rigid in the deuterium NMR time scale. Addition of $NADP^+$ in the ternary complex apparently hindered the librational motion of the methoxyl groups. T_1 and T_2 relaxation measurements also detected the presence of fast (>10^8 S^{-1}) and slow (< 10^3 S^{-1}) motions. The ionization states of folate analogues were studied with ^{15}N NMR. Our results showed that N5 of folate (HF) and dihydrofolate (H_2F) were not protonated at the pH range of 1.5 to 10. Addition of sodium dithionide at low pH causes a drastic change in the ^{15}N spectra of (5-^{15}N)H_2F. PK of N5 in this complex is estimated to be 2.3 ± 0.3. ^{15}N NMR of (5-^{15}N)HF and (^{15}N)H_2F in protein binary and ternary complexes showed that the N5 nitrogen is not protonated in the protein complex either. However, multiple conformations were detected in some of these complexes. ^{31}P and ^{17}O NMR have also been applied to detect the conformation of the protein complexes. Collectively these data suggests that ligand binding induces conformational changes such that significant shift of the phosphorous resonances were detectable. Results of these data will be discussed.

Tu-AM-D4

THE THREE-DIMENSIONAL SOLUTION STRUCTURE OF CALBINDIN D_{9k} IN THE CALCIUM-FREE AND CALCIUM-BOUND STATES.

Nicholas J. Skelton, Johan Kordel, Mikael Akke and Walter J. Chazin, Department of Molecular Biology, Research Institute of Scripps Clinic, La Jolla, CA 92037.

The principal long-term objective of structural research on the calmodulin superfamily of regulatory calcium-binding proteins is to identify the role of molecular conformation and dynamics in determining protein function and metal ion specificity. To fully understand the structural and dynamical consequences of Ca^{2+}-binding, specific binding domains must be examined in both the inactive (apo or Mg^{2+}-bound) and activated (Ca^{2+}-bound) states. Since it has not been possible to crystallize any member of this family of proteins with different levels of Ca^{2+} occupancy in a specific domain, the method of three-dimensional structure determination using ^{1}H NMR spectroscopy in solution is uniquely suited to solving this problem. The NMR method is being applied to examine native porcine and recombinant bovine calbindin D_{9k} in the Ca^{2+}-free and Ca^{2+}-bound states. Although the structures are in relatively early stages of refinement, we are now able to begin to formulate a view of the molecular events associated with the binding of Ca^{2+} by calbindin D_{9k}. The results are being analyzed with respect to the direct experimental evidence that reflect the changes in the structure and dynamics of the protein.

Tu-AM-D5

IDENTIFICATION OF INTERMOLECULAR CONTACTS BETWEEN α-BUNGAROTOXIN AND A BINDING-SITE PEPTIDE FRAGMENT OF THE NICOTINIC ACETYLCHOLINE RECEPTOR. Edward Hawrot and Vladimir J. Basus*, Section of Molecular and Biochemical Pharmacology, Brown University, Providence, RI 02912 and *Department of Pharmaceutical Chemistry, University of California, San Francisco, CA 94143.

Small synthetic peptide fragments derived from the α-subunit of the nicotinic acetylcholine receptor (nAChR) bind the curaremimetic, snake venom neurotoxin, α-bungarotoxin (BGTX), with μM affinity and thus serve as a useful model system for investigating the molecular determinants of BGTX interaction with the nAChR. We are using two-dimensional ^{1}H-NMR to determine the solution structure of the complex formed between BGTX (74 residues) and a dodecamer corresponding to residues 185 to 196 (KHWVYYTCCPDT) in the α-subunit of the nAChR from *Torpedo californica*. In order to eliminate any possible covalent interactions, the internal disulfide was formed between the adjacent Cys residues in the dodecamer and accurately reflects the fact that these Cys residues exist as a vicinal disulfide in the native nAChR. The ^{1}H-NMR spectra of mixtures of BGTX and the dodecamer added at various molar ratios clearly indicate that the complex is stoichiometric and is in slow exchange between the bound and free forms of BGTX and the dodecamer. In comparison to the previously determined ^{1}H-NMR resonance assignments for "free" BGTX, many resonances in "bound" BGTX have chemical shifts that are markedly perturbed indicating a significant change in chemical environment upon binding.

The assignment of the proton resonances for the entire complex is nearly complete and a number of intermolecular contact sites have been identified by Nuclear Overhauser effect (NOE) interactions between BGTX and dodecamer resonances. These NOE contact sites suggest that a hydrogen bond is formed between an imidazole-N in His-186 from the dodecamer and the hydroxyl of Tyr-24 in BGTX. His-186 also contacts Thr-6 and Ala-7 of BGTX. This set of interactions is consistent with the NMR solution structure of BGTX but is incompatible with the reported crystallographic structure. In addition, the methyl protons of Val-188 in the dodecamer are in contact with the methyls of Val-39 in BGTX and NOE-contacts are observed between His-68 in BGTX and Tyr phenol-ring protons in the dodecamer. Together, these NOE contacts define a cleft in BGTX formed by three segments of the toxin polypeptide chain that appears to be directly involved in recognition and binding to the nAChR.

Supported by NIH-GM32629 and the American Heart Association.

Tu-AM-D6

QUARTERNARY STRUCTURE IN THE PF-4 FAMILY OF PROTEINS MAY DICTATE BIOLOGICAL ACTIVITY. Gary CHEN, Sharon BARKER, and Kevin H. MAYO, Dept. of Chemistry, and The Fels Institute for Cancer Research & Molecular Biology, Temple University, Philadelphia, PA 19122.

To date, the PF-4 family of proteins includes: platelet factor-4 (PF-4); low affinity PF-4 (LA-PF-4; also called B-thromboglobulin or platelet basic protein); interleukin-8 (IL-8); growth related protein (Gro); Rous sarcoma virus-induced protein, and -interferon-induced protein. These proteins are primarily involved in inflammation response and immune regulation. Specific biologic activities of proteins in this family vary considerably. PF-4, for example, exhibits a high binding affinity for heparin, while LA-PF-4, which is an active mitogen and chemotactic agent, does not. We have investigated solution aggregation properties of PF-4, LA-PF-4, and IL-8 by using ^{1}H-NMR (500 MHz) spectroscopy. On a 500 MHz NMR time scale, relatively slow exchange exists among PF-4 and also among LA-PF-4 monomer/dimer/tetramer species, but not for IL-8 under the solution conditions studied. Equilibrium association constants, K_D and K_T, have been estimated from fractional populations derived from proton resonance integrals assigned to resonances in monomer/dimer/tetramer states. As a function of pH and ionic strength, K_D values for PF-4 and LA-PF-4 are similar, while K_T values differ significantly. Under near physiologic conditions, i.e., pH 7 and 0.1-0.2 M NaCl, PF-4 tetramer formation is favored, while LA-PF-4 monomer state is favored. Based on X-ray crystallographic data on tetramer bovine PF-4 (St. Charles, et al., (1989) J.Biol.Chem. 264, 2092), two types of dimers could form in solution, i.e., AB(CD) and AC(BD) types. Under dimer forming conditions, the thermodynamically favored dimer for PF-4 and LA-PF-4 is the AC type. IL-8, on the other hand, forms tightly associated AB type dimers. In the PF-4 family of proteins, quarternary structure, therefore, may dictate specific biological activity.

This work was supported by NIH grants (HL-43194; RR-04040) and by an American Heart Association research grant.

Tu-AM-D7

STRUCTURAL AND KINETIC STUDIES OF THE FAB FRAGMENT OF A MONOCLONAL ANTI-SPIN LABEL ANTIBODY BY NMR
Theriault, T.P., Rule, G.S., and McConnell, H.M.

Nuclear magnetic resonance has been used to study the structure of the anti-spin label antibody AN02 combining site and the kinetic rates for the hapten-antibody reaction. The association reaction for the hapten dinitrophenyl-diglycine (DNP-digly) is diffusion limited. The activation enthalpy for association, 5.1 kcal/mol, is close to the activation enthalpy for diffusion in water. Structural data deduced from the NMR spectra compare favorably with the crystal structure* in terms of the combining site amino acid composition, distances of tyrosine residues from the unpaired electron of the hapten, and residues in direct contact with the hapten. Evidence is presented that a single binding site region tyrosine can assume two distinct conformations on binding of DNP-digly.

The AN02 antibody is an autoantibody. Dimerization of the Fab fragments is blocked by the hapten DNP-digly. The NMR spectra suggest that some of the amino acid residues involved in the binding of the DNP-hapten are also involved in the Fab dimerization.

This work was supported by Office of Naval Research contract N00014-86-K-0388.

*Brünger, A.T., Leahy, D.J., Hynes, T.R., and Fox, R.O. in press.

Tu-AM-D8

THE 3D STRUCTURE OF THE ACTIVE INTERFACE BETWEEN RHODOPSIN AND G-PROTEIN DETERMINED USING 2D NMR. E.A. Dratz*, H.E. Hamm†, R. Zwolinski†, J. Furstenau* and C. Lambert*, *Dept. of Chemistry, Montana State Univ., Bozeman, MT 59717 and †Dept. of Physiology and Biophysics, Univ. of Illinois Med Center, Chicago, Il 60680.

Hamm and coworkers (Science, 241, 832-835, 1988) have shown that certain synthetic peptide segments of the retinal rod G-protein (transducin) can break up the active complex between photoexcited rhodopsin and the entire G-protein. Photoexcited rhodopsin exists in an equilibrium between the inactive, orange Metarhodopsin I (MI) and the active, yellow Metarhodopsin II (MII). Two different peptide segments of the G-protein, 340-350 and 311-329 directly interact with MII, pull the equilibrium away from MI and form a MII-peptide complex which stabilizes MII. The active peptides are in rapid exchange and have K_d near 1 mM. The 2D NMR spectra of the free peptides are assigned using TOCSY and ROESY. The structure of the active, MII bound conformation of 340-350 has been determined using transferred-NOE NMR (Tr-NOESY) combined with constrained molecular dynamics. Refinement of the structure is underway, and the structural model is being tested with peptide sequence variations predicted to increase or decrease the stability of conformational features. The method is being applied to the two other G-protein peptides and three rhodopsin peptides (Konig, et al, PNAS, 86, 6878-6882 (1989) that appear to make up the active interface between rhodopsin and G-protein. (Supported by NSF RII8921978, NSF DMB8804861, NIH EY06062, and Montana Center for Excellence in Biotech)

Tu-AM-D9

OFF-RESONANCE ROTATING FRAME SPIN-LATTICE RELAXATION: PROTON MAGNETIZATION TRANSFER IN EYE LENS.

G. H. Caines, T. Schleich, and J. M. Rydzewski, Dept. of Chemistry, Univ. of California, Santa Cruz, CA 95064.

The off-resonance rotating frame spin-lattice relaxation experiment represents a class of magnetic resonance techniques in which a low power, continuous wave radiofrequency (rf) field is applied off-resonance from a selected resonance, thereby establishing nuclear spin polarization along an effective field inclined at an angle Θ to the z-axis. We have extended the off-resonance rotating frame spin-lattice relaxation formalism to include the effects of magnetization transfer arising from either saturation transfer or cross relaxation. For a two component spin bath, such as tissue water protons (A) and macromolecular protons (B), the steady-state expression for the spectral intensity ratio of the A spin system incorporating magnetization transfer effects, but neglecting chemical exchange effects may be written as follows:

$$R^A = \frac{\left[R_A\left(\frac{R_T}{f} + R_B + \frac{1}{T_{e,B}}\right)\cos^2\Theta_A + R_B R_T \cos^2\Theta_B\right]}{D^{off}}$$

where R_A, R_T, R_B, and f represent, respectively, the spin-lattice relaxation rate constant of the A spins, the cross relaxation transfer rate constant, the spin-lattice relaxation rate constant of the B spins, and the ratio of B to A spins. The following definitions also apply:

$$D^{off} = R_A^{off}R_B^{off} + R_A^{off}\frac{R_T}{f} + R_B^{off}R_T\,, \quad \frac{1}{T_e} = \frac{T_2\omega_1^2}{1 + 4\pi^2\Delta^2T_2^2}\,, \text{ and } R_A^{off} = R_A + \frac{1}{T_{e,A}}\,.$$

Analogous expressions may be written for the B spin bath. The occurrence of cross relaxation in lens tissue was demonstrated by obtaining a lens water proton dispersion curve from an off-resonance radiofrequency irradiation experiment. Because of the dependence of the cross relaxation transfer rate on macromolecular dynamics, the view that water tissue proton relaxation times simply reflect the motional freedom of water molecules is erroneous. Much of the eye lens water proton relaxation data in the literature has been interpreted in terms of free and bound water fractions, thereby ignoring an appreciable relaxation contribution from the constituent lens protein protons. Current experiments are devoted to determining the variables which dictate and define lens water proton dispersion curve behavior in terms of lens protein motional dynamics. (Supported by NIH grant EY 04033)

Tu-AM-E1

A MODEL FOR THE FLUORESCENCE ANISOTROPY FROM DISKLIKE PROBES IN MEMBRANES WITH HINDERED IN-PLANE AND OUT-OF-PLANE ROTATIONS.

B. Wieb Van Der Meer [1], and Parkson L.-G. Chong [2]. (Introduced by Thomas P. Coohill) [1] Dept. of Physics and Astronomy, Western Kentucky University, Bowling Green, KY 42101, [2] Dept. of Biochemistry, Meharry Medical College, Nashville, TN 37208

Both the in-plane and out-of-plane rotations of perylene in membranes are hindered [Lakowicz *et al.*, Biochemistry 24(1985)376; Brand *et al.*, in "Spectroscopy and the Dynamics of Molecular Biological Systems", Bayley and Dale, eds. 1985]. A model is proposed that quantitatively describes these hindered rotations: We assume that there are two groups of planar probes in the membrane, one parallel to the surface of the membrane and the other perpendicular to the membrane. The first is situated near the center of the membrane and performs unhindered in-plane but no out-of-plane rotations, whereas the second group may be closer to the surface and undergoes isotropic out-of-plane and hindered in-plane rotational diffusion. Our experimental data indicate that the two fractions have different fluorescent lifetimes. We assign the longer lifetime to the first group with their planes parallel to the membrane surface. The total intensity has three parameters: the fraction x of probes perpendicular to the membrane surface, the longer lifetime of this fraction, and the shorter lifetime of the remaining 1-x. The fluorescence anisotropy has five additional parameters: the fundamental anisotropy r_0, the diffusion constant (or rate) of in-plane rotation, the diffusion constant (or rate) of out-of-plane rotation, and two order parameters. The order parameters refer to the degree of hindrance of the in-plane rotation: they are defined as $\langle\cos 2\psi\rangle$ and $\langle\cos 4\psi\rangle$, where the brackets indicate an ensemble average and ψ specifies the orientation of the planar probe in the group with the plane perpendicular to the membrane surface. It is assumed that the in-plane rotational diffusion constant for the two groups is the same. This model can explain the trends observed for time-resolved anisotropy from perylene in vesicles excited at positive r_0 and negative r_0 [Brand *et al.*, in "Spectroscopy and the Dynamics of Molecular Biological Systems", Bayley and Dale, eds. 1985]. This work is supported by NSF-MRCE.

Tu-AM-E2

STUDY OF CELL MEMBRANE MICRO-HETEROGENEITY USING FLUORESCENCE LIFETIME DISTRIBUTIONS

C. Ho[1], B.W. Williams[2] and C.D. Stubbs[1]
[1]Department of Pathology and Cell Biology, Thomas Jefferson University, Philadelphia, PA 19107 and [2]Chemistry Department, Bucknell University, Lewistown, PA 17837.

The use of DPH type fluorophores as probes of the protein-lipid interface in liver cell membranes was investigated using the continuous lifetime distribution model. A distribution of lifetimes is obtained when fluorophores exist in distinct environments while in the excited state, characterized by a distributional width at half-maximum. In membranes fluorophores may reside in two distinct regions while in the excited state, the bulk lipid and protein influenced regions respectively. This possibility was explored by analysis of the fluorescence decays as a trimodal distribution, to include the minor component typical of DPH type fluorophores.

For DPH-PC in membranes two major lifetime centers were obtained. One lifetime was attributable to fluorophores in the bulk lipid region and gave a zero distributional width, indicating a homogeneous environment. The other was due to the protein influenced region. DPH and TMA-DPH showed similar results in liver plasma membranes but in microsomes recovery of two distinct lifetime centers was not possible. This was due to the closeness of the two lifetime centers and the fact that both had a distinct distributional width in bulk lipids.

In principle the proportion of fluorophores influenced by protein can be obtained from the fractional intensity associated with the respective lifetime center. This can be used to calculate the number of protein influenced lipids for a particular protein, providing the protein:lipid ratio is known and the probe distribution follows that of the lipids. Using cytochrome b_5 in POPC vesicles this idea was tested and it was found that the number of protein influenced lipids corresponded exactly to the number of boundary lipids obtained from calculation and other studies. In summary using a trimodal distributional analysis of the fluorescence decay of membrane fluorophores, valuable information concerning the boundary lipid region of membranes can be obtained.

Tu-AM-E3

RED EDGE EXCITATION SHIFT IN MEMBRANES

Amitabha Chattopadhyay
Centre for Cellular & Molecular Biology
Hyderabad 500 007
India

Shift in the wavelength of maximum emission caused by shift in the excitation wavelength towards the red edge of the absorption band is termed the Red Edge Excitation Shift (REES). This effect is mostly observed with polar fluorophores in motionally restricted media such as very viscous solutions or condensed phases. Use of this effect in systems of biological relevance has so far been restricted mainly to fluorescent probes bound to proteins or to indole and tryptophan in viscous solvents. The focus of the current investigation is whether the phenomenon of REES takes place in highly organized molecular assemblies such as membranes. Results showing such red edge effects for membrane-bound probes and peptides will be discussed. Thus, gramicidin and NBD-labeled phospholipids when incorporated in model membranes of dioleoylphosphatidylcholine, show REES. Observation of REES in membrane is indicative of the fluorophore environment in the membrane. In addition, fluorescence polarization of these fluorophores in membranes shows excitation wavelength dependence with polarization increasing towards the red edge of the absorption band. REES thus appears to be a powerful tool for studying membrane dynamics.

Tu-AM-E4

PHASE TRANSITION KINETICS OF BINARY LIPID MIXTURE MEMBRANES

Qiang Ye and Rodney Biltonen
Biophysics Program, University of Virginia, Charlottesville, VA 22908

The relaxation kinetics of the gel-liquid crystalline transition of multilamellar vesicles made of binary mixtures of phosphatidylcholines have been studied with a volume-perturbation calorimeter. The temperature and pressure relaxations following a volume perturbation were used to moniter the transition time course. The data were analysed in the frequency domain using a Fourier series representation of the perturbation and response functions. In binary mixtures, the relaxation process consists of more than one exponential decay. This is in contrast to primarily single exponential decay observed in one-component systems. Since the volume-perturbation calorimeter measures the dynamic energetics, the relative energy contribution of each individual decay in a complex relaxation process is characterized by its thermal relaxation amplitude. The overall relaxation rate of binary lipid systems was found to be increased relative to pure lipid systems. The maximum relaxation time changed from about 3 seconds for pure DMPC MLV to about 0.006 seconds for a DMPC-DSPC MLV containing 6 mole% DSPC, a difference of almost three orders of magnitude. Two maxima in the relaxation times in the transition region were found for all 1:1 mixtures, although the equilibrium heat capacity function of these mixtures might have only one maximum as observed by differential scanning calorimetry. The maximum relaxation times appear at the temperatures where the modulus of the first derivative of the heat capacity is a maximum. Furthermore, mixtures with a small amount of lipid with higher melting temperature, T_m, in a dominant amount of lipid with lower T_m accelerates the transition dynamics much more dramaticaly than those with a small amount of lipid with lower T_m in a dominant amount of lipid with higher T_m. These results show that the compositional change in the lipid membrane can not only vary the transition temperature but also alters the thermodynamic fluctuation rates dramatically. (Supported by NIH GM37658 and ONR N00014-88-k-0326.)

Tu-AM-E5

LIPID ORGANIZATION IN PHOSPHATIDYLCHOLINE/[1-$^{18}O_2$]FATTY ACID MONOLAYERS PROBED BY LIPASE-CATALYZED ^{18}O EXCHANGE. J.M. Muderhwa, P.C. Schmid and H.L. Brockman, The Hormel Institute, University of Minnesota, Austin, MN.

Addition of carboxylester lipase (CEL) to the aqueous subphase below monolayers of ^{18}O-labelled docosadienoic acid ($^{18}O_2$-DA) results in CEL adsorption to the lipid-water interface and rapid exchange of both ^{18}O's with subphase $H_2{}^{16}O$. Exchange is monitored by GC/MS of recovered, methylated, hydrogenated and purified DA. Possible exchange mechanisms are $^{18}O,{}^{18}O$-DA $\xrightarrow{2k_2}$ $^{16}O,{}^{18}O$-DA $\xrightarrow{k_1}$ $^{16}O,{}^{16}O$-DA (random) and $^{18}O,{}^{18}O$-DA $\xrightarrow{k_1}$ $^{16}O,{}^{16}O$-DA (concerted). To assess the mechanism, the measured ratio $^{16}O,{}^{18}O$-DA/$^{18}O,{}^{18}O$-DA is divided by the expected random ratio, derived from the observed total % of ^{18}O exchanged, to give R. R is 1 for the random mechanism and 0 for the concerted. For CEL-catalyzed exchange of ^{18}O in monolayers of DA alone, R=0.90±.01. The rate expression for the random mechanism coupled with the observed linear time dependence of CEL adsorption is obeyed, yielding 2.7×10^{-5} cm sec^{-1} for the adsorption rate constant and 5.1×10^{-2} cm^2 $pmol^{-1}$ sec^{-1} for k_1.

Mixed monolayers of 1-palmitoyl-2-oleoyl-phosphatidylcholine and $^{18}O_2$-DA are liquid-expanded (chain melted) at 24°C. With such films, ^{18}O exchange for 30 nM [CEL] changes from near 0 to ~100% between 0.5 and 0.6 mol fraction of DA. With lower [CEL], R was measured as a function of [CEL], time and lipid composition. R was independent of [CEL] and time but changed from ~0.3-~0.9 between 0.5 and 0.6 mol fraction of DA, indicating a shift of mechanism. This suggests a change in surface structure with increasing DA. Moreover, the low values of R at low DA may not reflect a true concerted mechanism but the confinement of DA to 2-dimensional microdomains. R values near 1 and rapid ^{18}O exchange rates at high DA would reflect a high degree of connectivity of the DA domains and relative loss of film order. These results are consistent with reactant percolation being an important regulator of lipase activity in monolayers [Muderhwa, J.M. and Brockman, H.L. (1991) in press]. Support: NIH HL02003, NIH HL08214, & Hormel Foundation.

Tu-AM-E6

TRANSFER OF LIPID FROM VESICLES TO THE AIR-WATER INTERFACE: IDENTIFICATION OF SOME RATE-DETERMINING FACTORS. R. C. MacDonald, J. A. Farah, S. Chang and R. Qiu. Department of Biochemistry, Molecular Biology and Cell Biology Northwestern University, Evanston, IL 60208.

We have sought to define the relationship between half of a lipid bilayer and a lipid monolayer at the air-water interface. The chemical potential of molecules in the latter monolayer depends upon monolayer pressure, but there is one unique pressure, namely the equilibrium pressure, at which the chemical potential is the same for bilayer and monolayer. Although it appears that for unstressed liposomes, the equilibrium pressure must be the same as the monolayer collapse pressure, this may not be true for vesicles with high curvature (SUVs) or under osmotic or electrostatic stress. In the course of determining, using the Wilhelmy plate method, the monolayer surface pressure over suspensions of vesicles, we discovered that surface pressure of a freshly swept surface rose more rapidly, the larger ratio of Wilhelmy plate circumference to the monolayer surface area; the presence of the plate influences the rate of lipid transfer from vesicle to air interface. The magnitude of the plate effect depends upon its material in the order: nichrome> platinum> glass> paper. The manifestation of an effect of the plate is, moreover, strongly dependent upon the purity of the lipid. Commercially available samples of dioleoylphosphatidylcholine exhibited substantial variations in rates of transfer from vesicles to monolayer, the purest samples equilibrating most slowly. Addition of breakdown products such as lyso compounds or fatty acids to very pure phospholipids reproduced the same rapid transfer from vesicles to monolayer seen with commercial samples containing those impurities. Vesicles containing very large amounts of impurity generated high pressure monolayers rapidly even if the Wilhelmy plate was present only long enough to measure the surface tension. It remains to be determined whether or not the monolayer has the same composition as the vesicles in the cases of lipids containing impurities. Although vesicles of very pure dioleoylphosphatidylcholine do not generate monolayers with significant pressure over the course of hours, they do, as surface potential measurements reveal, spread in minutes to surface densities corresponding to a monolayer of lipid molecules lying on their sides (about 150 $Å^2$/molecule). Supported by NIH GM38244 and DK36634.

Tu-AM-E7

Simulation of the Molecular Mechanisms of the Formation of Cholic acid Micelles.

Wou-Seok Jou and Paul W. Chun, Dept. of Biochemistry and Moleculuar Biology, University of Florida, College of Medicine, Gainesville, FL 32610

The molecular mechanics of cholic acid micelle formations were simulated using the Sybyl energy minimization program (Maximm2) developed by Tripos Associates interfaced with micro-Vax.

Before energy minimization, the Cartesian coordinates a(x), b(y) and c(z) for the cholic acid dodecamer had values of 13, 18 and 6.7Å, respectively. After energy minimization, at 9,370 kcals/dodecameter, these values had increased to 21.6, 42.8 and 20.9Å. At an energy minimization level of 21,626 kcals/dodecamer, the micelle structure is stabilized by hydrophobic interaction, forming distinct horizontal channels along the b(y) axis, directing the carboxyl and hydroxyl groups toward the surface. These structural changes remain relatively constant as the process of energy minimization continues, down to the lowest energy level we considered, 9,370 kcals/dodecamer. The cholic acid layers are highly dissimilar, forming channels of irregular size, shape and orientation. Both the carboxyl groups and phenanthrene rings are in a puckered orientation which permits compact packing of the sandwiched multilayers.

From the dimensions of the channels, it is apparent that guest molecules such as phospholipid, cholesterol, or inorganic calcium can be incorporated into the micelle through more than one channel, forming inclusion complexes such as gallstones.

Tu-AM-F1

^{13}C Magic Angle Spinning NMR of the EF-Tu.GTP.aminoacyl-t-RNA complex labelled with [1-^{13}C]phenylalanine

H. de Groot, J. Raap and J. Lugtenburg
Dept. of Organic Chemistry
J.P. Abrahams, M. van Raaij and B. Kraal
Dept. of Biochemistry
Gorlaeus Laboratories, Leiden, The Netherlands.

With the Magic Angle Spinning (MAS) NMR technique it is possible to examine specific atoms in large macromolecular complexes by labelling them with dilute spin-1/2 nuclei, for instance ^{13}C. The esterification of [1-^{13}C]phenylalanine by $tRNA^{Phe}$ and the ~68 kD complex with EF-Tu.GTP are investigated with MAS NMR. This method has the advantage that the samples are frozen to ~190 K, which prevents degradation and dissociation of the complex. The contribution from the label is separated from the natural abundance background with (double) difference spectroscopy. A comparison with MAS results on [1-^{13}C]Phe and its methyl ester is given. It follows that the charge differences as observed with the NMR at the ^{13}C label are very small between the four species (<0.05 electronic equiv.). The esterification, however, clearly shows up in the variation of the chemical shift tensor, which reflects the symmetry changes in local electronic environment. The shifts are localized in the σ_{22} and σ_{33} elements, in agreement with model compound behavior. The broad resonance of the label in the EF-Tu.GTP.[1-^{13}C]Phe-$tRNA^{Phe}$ complex suggests variations in conformation in this complex.

Tu-AM-F2

DYNAMICS, STRUCTURE, AND FUNCTION ARE COUPLED IN THE MITOCHONDRIAL MATRIX.

Bethe A. Scalettar, James R. Abney, & Charles R. Hackenbrock. Department of Cell Biology & Anatomy, University of North Carolina, Chapel Hill, NC 27599-7090.

The coupling between metabolite diffusion and the structure and function of the mitochondrial matrix was explored using fluorescence anisotropy techniques and electron microscopy. To model metabolite diffusion, carboxyfluorescein was loaded into the matrix of intact rat liver mitochondria. The rotational diffusion of this fluorophore was then followed by monitoring its steady-state fluorescence anisotropy. Our data confirm that matrix ultrastructure and the concentration of matrix protein are influenced by the respiratory state of mitochondria and the osmolarity of the external medium. Under physiological conditions, carboxyfluorescein was found to diffuse slowly in the mitochondrial matrix but not to be completely immobile. In addition, significant differences in diffusive rates were found to exist between different mitochondrial respiratory states, with the slowest diffusion occurring in states with the highest matrix protein concentration. Taken together, these data support the concept of a matrix structure in which metabolite diffusion is considerably hindered due to limited metabolite-accessible water but are not consistent with the concept of a crystalline matrix. They further suggest that volume-dependent regulation of matrix protein packing may modulate metabolite diffusion and, in turn, mitochondrial metabolism.

This work was supported by NIH grant GM-28704 and NSF grant PCM 88-16611.

Tu-AM-F3

THE DNA IN HERPES SIMPLEX VIRUS CAPSIDS IS ARRANGED IN PARALLEL BUNDLES WITH AN INTER-DUPLEX SPACING OF 2.6nm.

F.P. Booy[1], W.W. Newcomb[2], B.L. Trus[1,3], J.C. Brown[2], T.S. Baker[4], and A.C. Steven[1].
[1] Lab. of Structural Biology Research, NIAMS, Bethesda, MD 20892; [2] Dept. of Microbiology and Cancer Center, Univ. of Virginia, Charlottesville, VA 22908; [3] Computer Systems Lab., DCRT, NIH, Bethesda, MD 20892; [4] Dept. of Biological Sciences, Purdue Univ., West Lafayette, IN 47907.

Cryo-electron microscopy and three-dimensional image reconstruction have been used to investigate the structural organization of HSV-1 DNA within the virus. Purified C-capsids, which are fully packaged, were compared with A-capsids, which contain no DNA. C-capsids show fine, often curvilinear, striations ("fingerprints") or quasi-hexagonal punctate arrays with a center-to-center spacing of ~ 2.6nm. This motif is not visible on A-capsids. Visualized in images from which the contribution of the capsid shell has been computationally filtered away, the encapsidated DNA does not exhibit icosahedral ordering. Instead, it is compacted into a uniformly dense ball, consisting of locally ordered parallel packings of duplex DNA that extend to a radius of ~ 43nm, i.e. right up to the inner surface of the icosahedral (T=16) capsid shell. The respective shells of A-capsids and C-capsids are indistinguishable in structure and molecular composition. The packing of encapsidated DNA in HSV-1 closely resembles that previously visualized in bacteriophages T4 and lambda (Lepault et al, EMBO J. 6:1507, 1987). These observations support the idea of a close parallelism between the respective capsid assembly pathways of a major family of animal viruses (the herpesviruses) and a major family of bacterial viruses (the dsDNA phages).

Tu-AM-F4

LOCALIZATION OF PROTEINS ON THE OUTER CAPSID SURFACE OF HERPES SIMPLEX VIRUS.

B.L. Trus[1,3], W.W. Newcomb[2], F.P. Booy[1], J.C. Brown[2] and A.C. Steven[1].
[1] Lab. of Structural Biology Research, NIAMS, Bethesda, MD 20892; [2] Dept. of Microbiology and Cancer Center, Univ. of Virginia, Charlottesville, VA 22908; [3] Computer Systems Lab., DCRT, NIH, Bethesda, MD 20892.

The most prominent features of the 15nm-thick icosahedral (T=16) capsid shell of HSV are hollow protrusions at the hexon and penton sites, and the "triplexes" - 3-fold-symmetric concentrations of density located at the trigonal sites between each set of three protrusions. In addition to the major capsid protein, VP5 (150 kDa), the shell contains several minor proteins that account for some 30% of its mass. In order to localize these proteins, with the goal of obtaining insights as to their functional significance, purified capsids have been treated with increasing concentrations of guanidine hydrochloride. Our initial results showed that, at 2M Guan.HCl, the shell protein, VP26 (12 kDa), as well as the core protein VP22 (46 kDa) (if present) are extracted, while electron microscopy of metal-shadowed capsids showed removal of the pentons (WWN and JCB - Manuscript in submission). We have now performed cryo-electron microscopy and three-dimensional reconstructions of both guanidine-extracted and control capsids. The results confirm that the pentons are extracted, and show that these sites are excavated to the deepest level of the capsid shell. Moreover, the extraction results in quantitative removal of the 120 peripentonal triplexes, while the other 200 edge- or facet-residing triplexes remain in place. Our current experiments are intended to allow a correlation between the biochemical and the structural information in order to effect a conclusive localization of these proteins.

Tu-AM-F5

REPLICATION AND PACKAGING OF BACTERIOPHAGE T7 DNA. Philip Serwer, Robert H. Watson, and Marjatta Son, Department of Biochemistry, The University of Texas Health Science Center, San Antonio, TX 78284-7760.

After their replication in vivo as a linear (in contrast to circular) molecule, intracellular bacteriophage T7 DNA molecules join end-to-end to form concatemers that are subsequently packaged in the T7 capsid and cut to mature size. Genetic removal of gene 6 exonuclease from T7-infected cells causes a degradation of T7 DNA that has the following characteristics: (a) DNA that is not linear (probably is branched) is cleaved to fragments that do not further degrade. (b) Degradation includes cleavage at most, but not all, regions of joining between genomes in concatemers. (c) Cleavage of these latter regions, but not most cleavage, is prevented by genetically blocking DNA packaging. (d) The remaining cleavage is prevented by genetically removing gene 3 endonuclease, specific for branched DNA. (e) The cleavage that requires gene 3 endonuclease includes some non-specific and some specific cleavage; specific cleavage at two known origins of late DNA replication was observed. From these observations, the conclusion is drawn that most degradation that occurs in the absence of T7 gene 6 exonuclease is caused by cleavage at branches. The following hypothesis is derived: Most, possibly all, of the additional branching caused by removal of gene 6 exonuclease is caused by strand displacement DNA synthesis at the site of RNA primers of DNA synthesis; the RNA primers, produced by multiple initiations of DNA replication, are removed by the RNase H activity of gene 6 exonuclease during a wild-type T7 infection. Observation of concatemerization in the absence of gene 6 exonuclease and additional observations indicate that the single-stranded terminal repeats required for concatemerization are produced by DNA replication. An observed selective, packaging-dependent shortening of the left end of T7 DNA in the absence of gene 6 exonuclease indicates that gene 6 exonuclease is required for formation of most, possibly all, mature left ends. Supported by NIH (GM24365) and the Robert A. Welch Foundation (AQ-764).

Tu-AM-F7

CONFIGURATION OF LIPOYL-BEARING DOMAINS IN PYRUVATE DEHYDROGENASE COMPLEXES. T. Wagenknecht, R. Grassucci, J. Berkowitz, G.A. Radke[1] and T.E. Roche[1]. Wadsworth Center for Laboratories & Research, New York State Dept. of Health and S.U.N.Y. School of Public Health, Albany, NY; and [1]Dept. of Biochemistry, Kansas State University, Manhattan, KS.

Pyruvate dehydrogenase complexes (PDC's) exist as large assemblies in which one of the component enzymes, dihydrolipoyl transacetylase (E2), forms a multisubunit core (24 or 60 E2 polypeptides per core depending on species) to which the other components bind noncovalently. The E2 polypeptides contain specialized domains which bind the lipoic acid cofactor. These lipoyl domains are thought to be attached to the E2 core via flexible, extended segments of polypeptide which allow them to function as swinging arms and to coordinate the sequence of reactions catalyzed by PDC. We are attempting to test this structural model by applying the technique of cryoelectron microscopy of frozen-hydrated specimens to isolated E2 cores and various chemically modified forms of the core. Image averaging of the E2 core from E. coli PDC shows that it is surrounded by a "halo" of faintly visible, apparently disordered material which extends more than 10 nm from the surface of the complex; this material likely corresponds to the lipoyl domains as its intensity is much reduced when the domains are removed by treatment with protease. Methodologies for labeling the lipoyl domains with probes (e.g. monoclonal antibodies, biotin-avidin) of sufficient size to be directly visible in electron micrographs are also being developed. Preliminary results from such studies on E2 cores from both E. coli and cow support the existence of extended, flexible tethers connecting the lipoyl domains to the E2 cores.

Tu-AM-F6

MODEL FOR MEMBRANE-MEDIATED ASSEMBLY OF FILAMENTOUS BACTERIOPHAGE Pf1

Raman Nambudripad[1], Wilhelm Stark[2], S.J. Opella[3] & Lee Makowski[1]

[1]Dept. of Physics, Boston University, Boston, MA 02215 [2]Biozentrum der Universitat Basel, Abteilung Strukturbiologie, CH4056, Basel, Switzerland, and [3]Dept. of Chemistry, University of Pennsylvania, Philadelphia, PA 19104.

The filamentous bacteriophage Pf1 consists of a large number of copies of a 46-residue major coat protein helically arranged around a single-strand of circular DNA. It assembles by a membrane-mediated process during which the DNA is secreted through the host membrane while being encapsulated by the major coat protein. Comparison of the conformation of the protein in the viral and the membrane-bound forms provides a basis for understanding the assembly process. Neutron diffraction of Pf1 with specifically deuterated amino acids was used to determine its structure in the intact virus. The coat protein consists of two α-helical segments arranged end-to-end with a mobile surface loop connecting the two helices. NMR was used to determine the structure in the membrane-bound form, where its secondary structure was found to be virtually unchanged. The mutual arrangement of the two helices was, however, found to be quite different, suggesting that during assembly of the virus particle, several hydrogen bonds form between the two segments. The conservation of the secondary structure coupled with changes in the tertiary structure may be a common principle in the assembly of membrane-associated macromolecules.